Ground-based Planetary Radars: Current and Future Prospects in the Cislunar Arena

T. Joseph W. Lazio[1]
Dimitrios Antsos[1], **Anthony Beasley**[2], **Lance A. M. Benner**[1], **Andrew Brooks**[1], **Marina Brozovic**[1], **Philip G. Edwards**[3], **Jon D. Giorgini**[1], **Shinji Horiuchi**[3], **Ed Kruzins**[3,4], **Clement Lee**[1], **Ronglin R. Liou**[1], **Blake Molyneux**[5], **Shantanu P. Naidu**[1], **Charles Naudet**[1], **Ryan S. Park**[1], **Chris J. Phillips**[3], **Marc Sánchez Net**[1], **J. Stevens**[3], **Mark Taylor**[1], **& Victor Vilnrotter**[1]
[1]*Jet Propulsion Laboratory, California Institute of Technology,*
[2]*National Radio Astronomy Observatory* [3]*CSIRO Space & Astronomy* [4]*UNSW Canberra Space*
[5]*Australia National University*

ABSTRACT

Ground-based planetary radars are used to conduct a variety of scientific observations of natural bodies across the Solar System, with a recent focus on near-Earth asteroids. The planetary science focus on near-Earth asteroids, which includes aspects of planetary defense, is to characterize their properties and determine their orbits. Some of these asteroids can approach within 1 lunar distance with sizes of order 10 m and radar cross sections that are 10% of their geometrical sizes. While the focus of ground-based planetary radars has been scientific, they also have been utilized for safety and mission assurance of high-value assets in low-Earth orbit (LEO) and in the recovery of spacecraft.

With an increasing focus on the cislunar arena, the utilization of the existing suite of ground-based planetary radars could be extended to that domain as well. In contrast to the typical asteroid observation, which is conducted in directions well separated from that of the Moon, cislunar radar observations have to account for the radiated emissions from the Moon. We describe a set of "use cases" that capture the range of potential observations that could be conducted and provide illustrations of capability. Further, we distinguish carefully between *detection* and *tracking*, which depend upon the extent to which an object's ephemeris is known.

We illustrate the system design for a future planetary radar capability that is based on an array of smaller antennas. Such a planetary radar array would be naturally scalable in capability, but also degrade gracefully. Therefore, it could have a sensitivity comparable to or exceeding that of the Arecibo Observatory, which collapsed in 2020, while also being able to access most of the sky much like the operational Goldstone Solar System Radar can.

We summarize the substantial recent progress toward producing large numbers of antennas with diameters of 15 m to 18 m and demonstrating the feasibility of kilowatt-level solid-state transmitters and amplifiers that could be used in such an array.

1. INTRODUCTION AND MOTIVATIONS

There is a long history of using powerful ground-based transmitters to conduct *planetary radar* observations of Solar System bodies (Figure 1). These planetary radar observations have been used to probe the surfaces of all of the planets with solid surfaces and many smaller bodies in the solar system, delivering information on their spin states and shapes, improving the knowledge of their (heliocentric) orbits with high-precision radar astrometry, and measuring dielectric properties of their (near-sub) surfaces [27, 30, 28, 29]. The prime use for the ground-based planetary radar infrastructure for over the past decade has been to observe near-Earth asteroids (NEAs). In addition to characterizing the objects, orbit determinations have played a key role in mission design and navigation of spacecraft to asteroids and assessing Earth-impact probabilities. (Ostro & Giorgini [31] and Giorgini et al. [11] provide a quantitative assessment of these observations with a specific focus on orbit determination.) The importance of ground-based planetary radar observations was recognized by multiple findings in the recent National Academies' *Origins, Worlds, and Life* Decadal Survey report.

Goldstone Solar System Radar
70 m antenna, 450 kW transmitter, 4 cm wavelength

Green Bank Telescope
100 m antenna, *currently receive-only*

Arecibo Observatory

Canberra Deep Space Network DSS-43
70 m antenna, 80 kW transmitter, 4 cm wavelength
+ Australia Telescope Compact Array
receive only

Fig. 1: The ground-based planetary radar infrastructure has enabled a variety of discoveries about all of the terrestrial planets, the Galilean moons of Jupiter, the rings of Saturn, and near-Earth asteroids. This infrastructure also has been used to conduct statistical studies of orbital debris and track and recover lost spacecraft. (Managing or operating institutions are noted parenthetically.) While the Arecibo Observatory is no longer operational, there continue to be scientific results produced from data acquired previously, and it serves as a benchmark against which to compare possible future capabilities. (Credits: Deep Space Network [DSN]/NASA; Green Bank Observatory [GBO]; Arecibo Observatory; CSIRO Radio Astronomy Image Archive)

The Goldstone Solar System Radar observes about 40 NEAs per year, most of which approach within 0.1 au (1.5×10^{10} m) and are at least a few hundred meters in diameter. Of these, at least a dozen objects per year are targets-of-opportunity, usually small NEAs, tens of meters in size, approaching within a few lunar distances. One of the smallest NEAs ever observed was 2006 RH_{120}, with a diameter of approximately 2 m, that was captured temporarily in Earth's orbit from 2006 July to 2007 July. This NEA was the first of two "minimoons" identified to date.

In addition to studying planetary bodies, ground-based planetary radars are used for aspects of NASA safety and mission assurance (SMA). In low-Earth orbit (LEO), operational spacecraft and astronauts face risks from impacts of "orbital debris," which range from meter-scale objects such as non-operational spacecraft to sub-millimeter–scale objects such as flecks of paint. In the most extreme case, orbital debris impacts could lead to catastrophic failure of an operational spacecraft or the death of an astronaut. Radar measurements are one of the standard data sources used in risk assessments conducted by the NASA Orbital Debris Program Office (ODPO) [19, 17, 12].

Extending beyond LEO, ground-based planetary radars have been used to track spacecraft in the cislunar arena and beyond. Notable examples include the recovery of the Solar and Heliophysics Observatory (SOHO),[2] for which the ground-based radar determined the spacecraft attitude; the confirmation that the (defunct) Chandrayaan-1 spacecraft[3] was still in orbit [3]; and the observations of objects classified originally as NEAs and later recognized to be defunct spacecraft.[4] The experience with observing small, closely approaching NEAs, in part, motivated studies of radar observations of cislunar spacecraft such as Chandrayaan-1.

[2] "SOHO spacecraft located with ground-based radar,"
`https://sohowww.nascom.nasa.gov/newsroom/oldesapr/press27.html`

[3] "New NASA Radar Technique Finds Lost Lunar Spacecraft," `https://www.jpl.nasa.gov/news/news.php?feature=6769`

[4] "New Data Confirm 2020 SO to be the Upper Centaur Rocket Booster from the 1960's,"
`https://www.nasa.gov/feature/new-data-confirm-2020-so-to-be-the-upper-centaur-rocket-booster-from-the-1960-s`

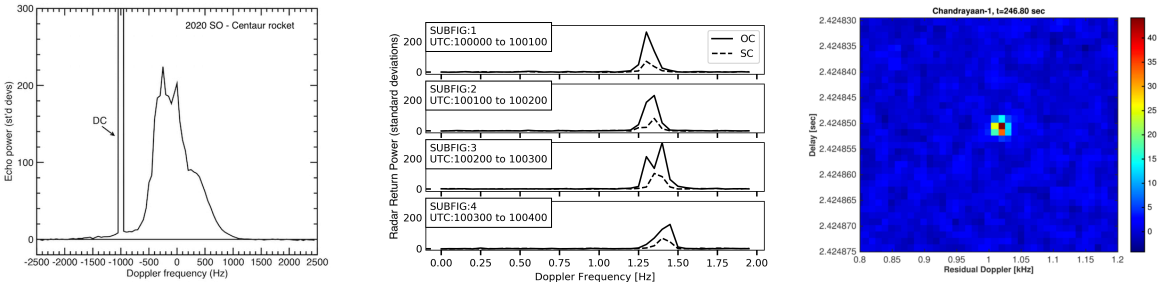

Fig. 2: Recent radar observations at cislunar distances. In all examples, the frequency width of the return can be used as a measure of the object's rotation while the offset from 0 Hz can be a measure of how well known the object's ephemeris is. (*right*) 2020 SO, "discovered" as a near-Earth asteroid, it was recognized soon thereafter as likely to be a defunct rocket booster. At the time of this observation, the object was at approximately 2.4 lunar distances. (*middle*) Near-Earth asteroid 2019 GC_6. Based on its brightness at visible wavelengths, its size is estimated to be 15 m, which suggests a radar cross-section of about 1.5 m for typical asteroid radar albedos. At the time of observations, this object was at approximately 0.6 lunar distances. The four panels show successive one-minute integrations, with the solid lines in each panel showing the radar return in the sense of polarization opposite that which was transmitted (OC) and the dashed lines showing the radar return in the same sense of polarization (SC). The changes in the width of the radar return signal likely reflects rotation of the object, while the differences in the power levels between the two polarizations indicate properties of the asteroid's surface. (*right*) Recovery of the lunar-orbiting Chandrayaan-1 spacecraft, shown as power as a function of both time-delay (range) and the residual Doppler shift. For orbit determination purposes, the effective range resolution is 37.5 m per pixel and the Doppler shift resolution is 10 Hz. (From Brozović et al. [3])

As activity increases in the cislunar arena, both robotic and crewed, the need for spacecraft tracking and "orbital debris" assessments is expected to increase, and there is the possibility for continuing this synergy of scientific observations and SMA activities (Figure 2). In particular, there is an expectation that larger numbers of small spacecraft (SmallSats) of meter- or sub-meter–sizes could be present in the cislunar arena. As these SmallSats reach the end of their operational lives (or fail), they may present challenges in maintaining knowledge of their orbits to ensure that there are no risks to operational spacecraft, particularly those for crewed missions.

In the remainder of this paper, we describe "use cases" that have been identified in an on-going set of studies focused on extending SMA capabilities to the cislunar arena, summarize the current capabilities, then look to a potential future means of improving upon the current capabilities. Throughout, we take 1 lunar distance (1 LD) to be 384,400 km.

2. CISLUNAR RADAR USE CASES

Table 1 illustrates cislunar radar use cases that we have identified and provides some measure of current or near-term capability. We distinguish between two aspects of these use cases:

Track The objective is to obtain a radar return from a target for which the ephemeris is known in advance and do so with sufficient signal-to-noise (S/N) ratio to (i) Confirm from the target's Doppler shift, and ideally a measurement of its range, that the ephemeris has not changed, or (ii) Use the target's Doppler shift, and ideally a measurement of its range, to update the ephemeris. This kind of radar observation is the standard for scientific observations of NEAs.

Detect The objective is to obtain a radar return from a target with no (or minimal) advance knowledge of its ephemeris with sufficient S/N ratio to obtain at least the target' Doppler shift and ideally a measurement of its range.

These two aspects, tracking vs. detection, should be viewed as extremes among a range of possibilities. For instance, in general, the precision to which the ephemeris of a target needs to be known depends upon its radar cross section—targets with large radar cross sections can be detected with more poorly known ephemerides than targets with small radar cross sections.

Table 1: Cislunar Radar Use Cases

Use Case	**Capability**	
	Detect	**Track**
Target far from Moon in angular separation (much farther than diameter of transmit or receive antenna beams)	*2-m*	0.6-m
Target $>$ 1 lunar radius in angular separation but receive beam overlaps Moon by 25%	3 m	1 m
Target $>$ 1 lunar radius in angular separation but receive beam overlaps Moon by 50%	*4 m*	*1.5 m*
Target in front of the Moon (projected separation from center of Moon $<$ 1 lunar radius or Moon 100% in beam)	*6 m*	*2 m*

Notes: These values assume a Goldstone Solar System Radar-like system (Table 2) for both transmitting and receiving, with an assumed time-bandwidth product of 1 s·1 Hz for detection and 100 s·1 Hz for tracking. A radar albedo of 10% is assumed, characteristic of asteroids, and a signal-to-noise ratio of 10 is required for both cases. A normal font is used to indicate use cases for which experiments have obtained results consistent with the projections, though the actual experimental systems have varied; an italic font is used for projections based on demonstrations to date.

We expand briefly upon these various use cases, and Figure 3 illustrates two aspects of intermediate uses cases. First, two spacecraft were targeted in the experiment illustrated, one with a well-known ephemeris (Lunar Reconnaissance Orbiter [LRO]) and one with only an approximately known ephemeris (Chandrayaan-1). Second, both spacecraft were "close" to the Moon, but neither was in front of the Moon during the radar observation. (These two examples are among those that confirm the projected performance from the second row of Table 1.)

The case of a *target far from Moon in angular separation* is the standard case for NEAs. As described above, these are typically much more distant than the Moon, but there are objects that approach within 1 LD. Moreover, there are orbits that can carry spacecraft far from the Moon. An exemplar of such orbits is a near-rectilinear halo orbit (NRHO), which is used currently by the Cislunar Autonomous Positioning System Technology Operations and Navigation Experiment (CAPSTONE) CubeSat and is the planned orbit for NASA's Lunar Gateway. Spacecraft in this orbit are approximately at 1 LD, but can extend as far as 70,000 km away from the Moon, equivalent to approximately 10° in angular separation from the Moon.

The case of a *target in front of Moon* is challenging in two respects. First, the Moon radiates at radio wavelengths, producing an effective additional noise contribution and leading to a reduction in sensitivity for the receiving system, an effect that is well known for communication applications [20, 21]. (Formally, the receiving system noise temperature increases, viz. §3, eqn. 2 and following text.) For radar observations, the closer that the target is to the Moon, the larger its radar cross section must be in order to maintain a comparable S/N ratio, all other things being equal. Second, the radar cross section of the Moon is so large that it will result in a radar return, which must be distinguished from that of the target.

With respect to distinguishing between the radar returns of the target and the Moon, there are two possible sub-cases. One possibility is that the target is in a relatively low altitude orbit, e.g., the LRO is on an orbit for which its altitude varies from as low as approximately 20 km to more than 150 km. These orbits are challenging from a radar perspective because the time delay between the target and the Moon is small ($\sim$ 0.3 ms). Thus, there is significant power in the radar return from the Moon, with the challenge of separating it from that of the target.

A second possibility is that the target is well in front of the Moon, for example, near the Earth-Moon Lagrange point 1 (L1), which is approximately 50,000 km in front of the Moon (equivalent to approximately 2×0.17 s round-trip light-travel time). For these targets, separation of the radar returns from the Moon and the target is much more feasible.

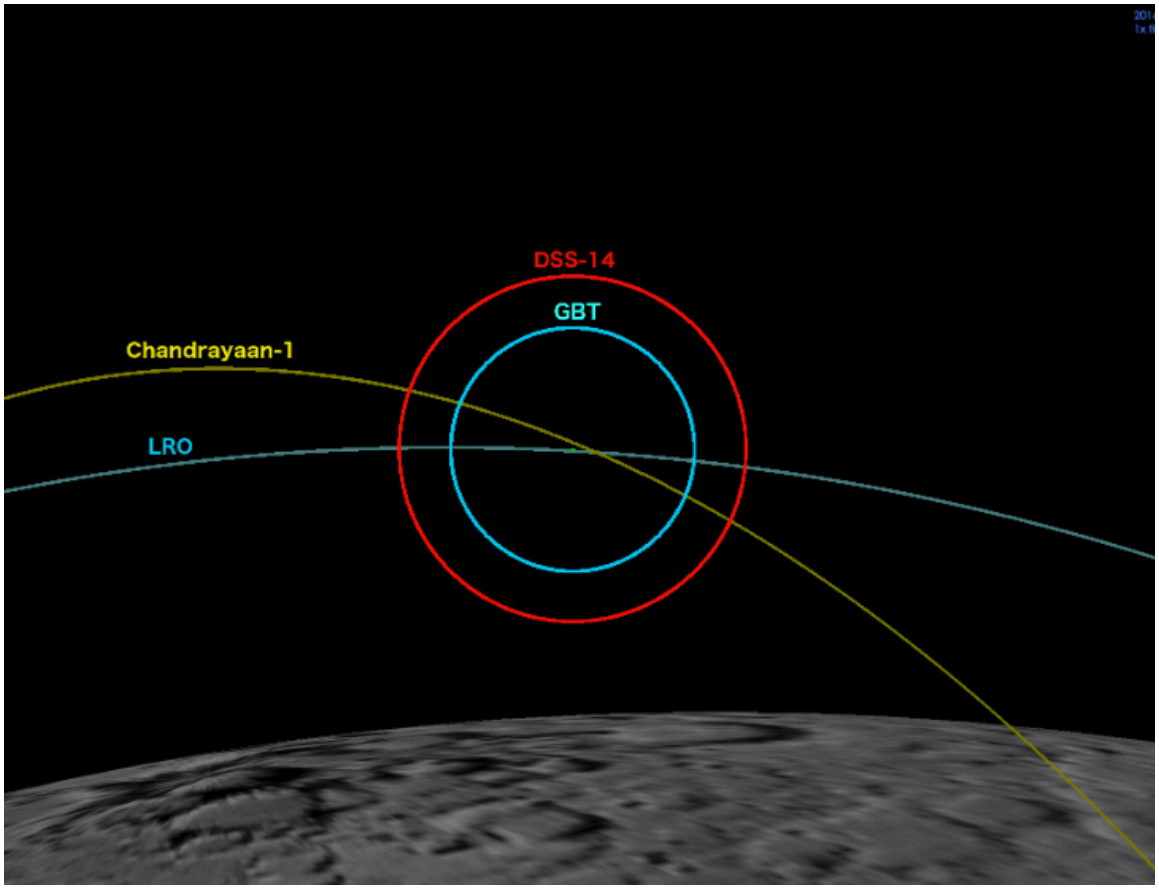

Fig. 3: Illustration of an intermediate cislunar radar use case. The Moon's limb is visible in the lower portion of the figure. The transmit beam of Deep Space Station-14 (DSS-14) is the red circle, and the receive beam of the Green Bank Telescope (GBT) is the cyan circle; these antennas are described further in §3. The orbit of the Lunar Reconnaissance Orbiter (LRO) is the light blue curve, and the orbit of Chandrayaan-1 is the yellow curve. In this experiment, sensitivity of the GBT was affected because it was pointing close to the Moon, and the ephemerides of LRO was well known while that of Chandrayaan-1 was only approximately known. (From Brozović et al. [3].)

3. CURRENT GROUND-BASED PLANETARY RADAR CAPABILITIES

Table 2 summarizes the current ground-based planetary radar capabilities, with a focus on the transmitting capabilities. The primary facility for ground-based planetary radar observations is the **Goldstone Solar System Radar** (GSSR), either operating monostatically or bistatically with a separate receiving asset, which both has the highest power transmitter and can observe approximately 75% of the sky. Over the past decade, an initial **Southern Hemisphere** capability, formed by a *bistatic* combination of the 70 m Deep Space Station-43 (DSS-43) antenna at NASA's Deep Space Network (DSN) Canberra Complex and the Australia Telescope Compact Array (ATCA) has been demonstrated [1, 13]. The **Green Bank Telescope** is equipped currently only for reception, but there is a funded effort to develop a transmitting capability for it. Naidu et al. [24] provide further technical details and comparisons between the various facilities, but, notably, most of this observational capability is based in the United States.

The systems in Figure 1 and Table 2 reflect the challenges associated with obtaining sufficient signal-to-noise ratios for targets in the cislunar arena and beyond. Specifically, the signal-to-noise ratio obtained at a receiving system, from a radar waveform transmitted by a transmitting system, is

$$\mathrm{S/N} = \frac{P_{\mathrm{RX}}}{\Delta P}\sqrt{\Delta\nu\Delta t}, \tag{1}$$

where P_{RX} is the power received by the receiving system, ΔP is the noise in the receiving system, and $\Delta\nu\Delta t$ is the

Table 2: Planetary Radar Infrastructure

System	Antenna	Transmitter Power	Transmit Frequency / Wavelength	Transmit Gain	EIRP
Goldstone Solar System Radar	70 m diameter	450 kW	8.56 GHz 3.5 cm	73.7 dBi	11 TW
Green Bank Telescope	100 m diameter	*∼ 500 kW proposed*	*13.9 GHz 2.1 cm*	81.0 dBi	
Southern Hemisphere	70 m diameter transmit +50 m equivalent receive	80 kW	7.19 GHz 4.2 cm	72.5 dBi (TX) / 92 dBi (RX)	1.4 TW
Deep Space Station-13 (Goldstone)	34 m diameter	80 kW	7.19 GHz 4.2 cm	67.0 dBi	0.4 TW

Notes: The gains listed assume that the system is used in a *monostatic* mode, in which the same antenna transmits and receives, such that the gains are the same. The exception is that the Australia Telescope Compact Array (ATCA) is used for receiving in the southern hemisphere. Its antennas are reconfigurable. The listed value assumes a maximum antenna separation of 750 m; larger separations would have higher gains.

bandwidth-time product for the observations. In turn, the received power is determined by the radar equation,

$$P_{\rm RX} = \frac{1}{4\pi} G_{\rm RX} [P_{\rm TX} G_{\rm TX}] \lambda^2 \left[\frac{\sigma}{(4\pi)^2 R^4} \right], \tag{2}$$

where $G_{\rm RX}$ is the gain of the receiving system, $G_{\rm TX}$ is the gain of the transmitting system, $P_{\rm TX}$ is the power transmitted by the transmitting system, λ is the observational wavelength, σ is the radar albedo or the radar cross section, and R is the range or distance to the target. The notable factor of R^{-4} in the radar equation can be considered to be the consequence of Huygen's Principle—the transmitted signal suffers an R^{-2} loss by the inverse-square law in traveling to the target, the illuminated surface of the target then reradiates this signal, which suffers an additional factor of R^{-2} loss upon its return to the receiving antenna.

We now consider the various factors in eqns. (1) and (2), distinguishing between those that are available for optimization or under the control of the observer and those that are properties of the target and not under the control of the observer.

- The noise power in the receiving system is $\Delta P = k_B T_{\rm sys} \Delta\nu$, where k_B is Boltzmann's constant ($1.380\,649 \times 10^{-23}\,{\rm J\,K^{-1}}$), the system temperature is $T_{\rm sys}$, and the receiver bandwidth is $\Delta\nu$. These factors would seem to be under the observer's control. However, in practice, a well-designed system will use cryogenic receivers from which the noise contribution is approaching fundamental limits. A typical value at the relevant frequencies, for a target far from the Moon in angular separation is $T_{\rm sys} \approx 25\,{\rm K}$, though, as discussed in §2, the Moon's natural radiation can be considered to contribute to $T_{\rm sys}$ and pointing close to the Moon can lead to substantially higher values (as much as 200 K, or poorer sensitivity). Finally, optimized performance is obtained when the receiver bandwidth $\Delta\nu$ is well-matched to the *Doppler bandwidth* of the target, a topic to which we return below. In practice, modern receiving systems can obtain values of $\Delta\nu$ that are comparable to or higher resolution than the Doppler bandwidth of the target.

- For an antenna of diameter D with aperture efficiency ε operating at a wavelength λ, the antenna gain is $G = 4\pi A_{\rm eff}/\lambda^2$, with the antenna's effective aperture being $A_{\rm eff} = \varepsilon\pi(D/2)^2$. Importantly, current single-dish antennas are at the scale that larger antennas are not a viable approach to obtain substantial improvements in antenna gain: No fully-steerable single dish antenna significantly larger than the GBT has since been constructed since its completion in the early 2000s. We return to this point in §4.

- Radar experiments are conducted in both *monostatic* and *bistatic* configurations. In a monostatic experiment, the same antenna is used both to transmit and receive, $G_{\rm TX} = G_{\rm RX}$. A prime benefit of monostatic experiments is simpler logistics, observations at only a single antenna have to be scheduled as opposed to coordinating observations at two antennas. In a bistatic experiment, different antennas are used for transmitting and receiving. While potentially more challenging from the perspectives of scheduling, the observations are easier at each antenna, which either transmits or receives instead of switching between the two. Indeed, the mechanisms for switching between transmit and receive typically are the limiting factor in determining whether a monostatic experiment is even possible: If the switching mechanism takes longer than the round-trip light travel time to the

target, it simply is not possible to switch between transmit and receive. Historically, the switching time scales for both the Arecibo Observatory and the GSSR have been longer than 1 s, meaning that observations of objects closer than the Moon have required bistatic observations.

- The optimum receiving bandwidth, in the bandwidth-time product of eqn. (1), is one that is matched to the Doppler bandwidth of the target, $\Delta\nu \propto d/(\lambda P)$ for an object with a diameter d and rotational period P. Modern systems can obtain bandwidths of 1 Hz or better, allowing the received signal to be well-matched to the Doppler bandwidth.

- The integration time, in the bandwidth-time product of eqn. (1), depends upon the characteristics of the target and the extent to which its ephemeris is known. For objects with well-determined ephemerides and that are being observed to characterize their properties, integration times could exceed the round-trip light travel times significantly. By contrast, if the purpose is a detection experiment to assess whether an object is on some orbit, the integration time should not exceed the time it takes for the object to pass through the transmit or receive beams, whichever is smaller. (For example, for the detection experiment such as that illustrated with Chandrayaan-1 in Figure 3, the integration time should not exceed the interval that the spacecraft had spent within the GBT beam.)

- A common metric for the performance of a radar system, particularly applicable for bistatic experiments, is the *effective isotropic radiated power* $\mathrm{EIRP} = G_{\mathrm{TX}}P_{\mathrm{TX}}$. While we use the EIRP of systems as a metric (Table 2), there are alternate formulations that parameterize systems by $\mathrm{EIRP}/\sqrt{\Delta\nu}$.

All of the systems listed in Table 2 have an operational or planned transmitting capability. Two other key (receive-only) facilities that have been used in a number of bistatic radar observations are the Very Large Array (VLA, [23, 22, 35, 9]) and the Very Long Baseline Array (VLBA, [5, 6]). There also have been limited experiments with a variety of other antennas used, largely for reception (e.g., [10, 26]). Further, there are two (receive-only) facilities likely to be available in the 2030s that could provide substantially higher values for G_{RX} than are available currently for bistatic radar observations. The **Square Kilometre Array Phase 1 (SKA1-Mid)**, to be sited in South Africa, is planned to be capable of receiving at the transmit frequencies of the DSN's Canberra Complex [16], but there will be only limited common sky visibility. In the northern hemisphere, the proposed **next-generation Very Large Array (ngVLA)**, when operational in the 2030s, would offer frequency coverage that overlaps with the GSSR (and a GBT transmitter system, if implemented) and considerable mutual visibility [2].

4. A FUTURE PLANETARY RADAR ARRAY

As illustrated in Figure 1, the traditional approach to compensate for the R^{-4} factor in the radar equation (eqns. [1] and [2]), has been to construct large-diameter monolithic antennas with large gain G and equipped with powerful transmitters.[5] At the time that the first planetary radar systems were constructed, this architecture was reasonable, but the steadily decreasing cost of electronics has led to an array architecture becoming increasingly competitive.

The concept of an antenna array is simple: Combine the signal transmitted and/or received by a collection of "small" antennas in such a way that the total system performance is equal to that of a much larger monolithic antenna. It does require careful design and implementation of the signal processing and electronics components to achieve the theoretical arraying gain, but it is now the standard approach for (receive-only) radio astronomy telescopes.[6] Moreover, radio astronomical arrays have been used to receive radar transmissions [23, 22, 35, 9, 42], and the ATCA is a standard part of the Southern Hemisphere system (Table 2).

Several reasons motivate a focus on an array of ground-based antennas for a future planetary radar system: First, large monolithic antennas are expensive to build, operate, and maintain, especially when large sky coverage is required. Several independent studies have evaluated the trade between antenna diameter and number of arrayed antennas [36, 18, 4, 33, 34]. Consistently, they have shown that large monolithic antennas have a significantly larger life-cycle

[5] An alternate approach, not considered here, is to place either the transmitter or receiver close to the target body, thereby modifying eqn. (2) to have an approximately R^{-2} dependence. This approach does have some advantages, but also disadvantages that need to be evaluated carefully such as spacecraft lifetime and accessibility to targets of interest.

[6] Sir Martin Ryle shared the 1974 Nobel Prize in Physics for his efforts to develop the techniques related to the use of multiple antennas in radio astronomical arrays.

cost than arrays of smaller antennas, a conclusion that is reflected in actual practice as the DSN and other ground-based science observatories (e.g., the Very Large Array [VLA], the Very Long Baseline Array [VLBA], the Australia Square Kilometre Array Pathfinder [ASKAP], the Karoo Array Telescope [MeerKAT]) have invested in technologies associated with arraying antennas. It is also notable that, with the exceptions of the Sardinia Radio Telescope (SRT, 65 m) and the Qitai Radio Telescope (QTT, planned 110 m), large-diameter, *fully-steerable* radio telescopes generally are not planned for future radio telescopes; the Five-hundred meter Aperture Spherical Telescope (FAST), while the largest single radio aperture, is limited in the fraction the sky that it can observe, as its architecture is similar to that of the former Arecibo Observatory. Second, arrays of antennas offer significant advantages in terms of capability degradation due to the planned or unplanned maintenance, so-called "graceful degradation." Indeed, when a large monolithic antenna needs to be serviced, the entire system capability is temporarily lost. In contrast, an array of antennas simply experiences a temporary service degradation, which can be shown to be increasingly small as the number of array elements increases.

For illustration, examples of recently commissioned and planned radio astronomy arrays operating at frequencies relvant to planetary radar include ASKAP (36 $\times$ 12 m-diameter antennas, [14]), MeerKAT (64 $\times$ 13.5 m-diameter antennas in South Africa, [15]), the SKA1-Mid[7] (expanding MeerKAT with 133 $\times$ 15 m-diameter antennas, *planned*), and the ngVLA[8] (244 $\times$ 18 m-diameter antennas in North America, *planned*).

Considerable design work and proof-of-concept demonstrations have been conducted for an "uplink" antenna array, primarily in the context of spacecraft commanding for the DSN [37, 8, 7, 38, 39, 40], though Vilnrotter et al. [41] also illustrated (delay-Doppler) imaging of planetary bodies. Most recently, Sánchez Net et al. [32] describe the system architecture of a planetary radar array and present the optimization for achieving maximum performance at a minimum of life-cycle cost.

Finally, because an antenna array is specified using two degrees of freedom—the number of elements in the array and the gain of each element—it can be designed to optimize both sensitivity and sky coverage. Consider the case of the Arecibo Observatory and the GSSR, both monolithic systems: While the former was 15 times more sensitive than the latter, it could only survey 32% of the accessible sky, compared to 79% for the GSSR [24]. An array of ground antennas can be designed to achieve the sensitivity of the Arecibo Observatory as well as the sky coverage of the GSSR.

The system architecture described by Sánchez Net et al. [32] has four, high-level sub-systems: the *Array Element*, *Signal Processing*, *Array Services and Infrastructure*, and *Operations Computing and Software*. Our focus here is on a subset of the full system architecture, as many elements have straightforward analogs to those used currently within ground-based radio astronomy arrays or the DSN. For more extensive discussion of other elements, the reader should consult Sánchez Net et al. [32]. Finally, our focus here is on the physical infrastructure, but the "concept of operations" for a planetary radar array likely could incorporate significantly more automation than has been used to date in the existing systems.

4.1 Array Element: Mechanical Antenna

Figure 4 illustrates the range of antenna diameters that were considered. The design and construction of radio antennas is a mature field. Key considerations for the optimization were that the range of diameters encompassed the likely optimum diameter, given past experience in designing arrays, and that the antenna likely could be manufactured in the necessary quantities on a reasonable time scale.

4.2 Array Element: Transmit System

For over a century, vacuum tube amplifiers have served as the standard source for high-power radio frequency (RF) signals used in communications and radar transmitter systems. Notably, the klystrons used in planetary radar applications have produced hundreds of kilowatts of power (250 kW to 500 kW, Table 2), and, unlike many other radar implementations, the standard approach for planetary radars (the GSSR and the former Arecibo Observatory) is that klystrons are operated in a continuous wave mode, rather than a pulsed mode.

These klystrons have presented multiple challenges associated with their often limited lifetime and reliability. Klystrons amplify a small input signal using a high-density electron beam. Beam formation requires the use of a high-potential electron gun, and this high-voltage requirement adds size and complexity to the transmitter and associated power

[7] `https://www.skao.int/en/science-users/118/ska-telescope-specifications`
[8] `https://ngvla.nrao.edu/page/refdesign`

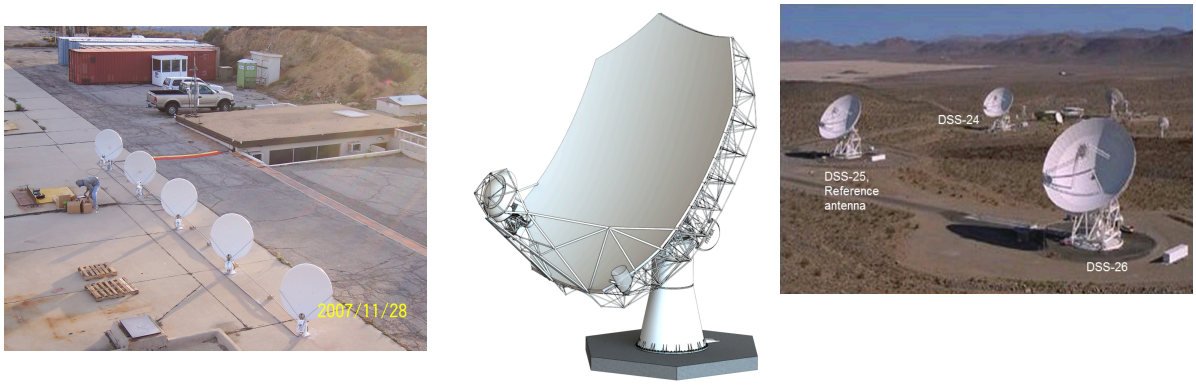

Fig. 4: Range of possible antenna diameters considered in the design and optimization of a planetary radar array. (*left*) Loop Canyon array, five 1.2 m diameter antennas. (From D'Addario et al. [7]) (*middle*) next-generation Very Large Array (ngVLA) antenna, an 18 m diameter antenna that would be used in the 244-element ngVLA; a prototype antenna is scheduled to be constructed starting in 2023. (Credit: mtex/NRAO/AUI/NSF) (*right*) "Apollo site" 34 m diameter antennas at the Goldstone Deep Space Communications Complex, not shown in this figure is a fourth antenna currently under construction.

supply. Additionally, typical klystron efficiency does not exceed 50%. When coupled with the large power densities within the electron beam, localized heating tends to limit lifetime and reliability for the high power klystrons, particularly at higher frequencies.

Though vacuum tube amplifiers are not likely to disappear anytime soon, recent advances in solid-state amplifier technology provide a potential alternative for a planetary radar array (Figure 5). While individual solid-state transistors are orders of magnitude lower in output power compared to tube amplifiers, techniques for combining many of these devices in parallel exist. Notably, a 30 kW system operating at approximately 7 GHz has been implemented at the Misasa Deep Space Station of the Japan Aerospace Exploration Agency (JAXA) [25]. While systems with tens of kilowatts have a much lower EIRP than the GSSR, with its dual 250 kW klystrons, leveraging substantial commercial investment in solid-state transmitting systems could produce a planetary radar array with capabilities comparable to or exceeding those of the GSSR or the former Arecibo Observatory.

4.3 Calibration

A critical element of a radar array is that it be phased. The requirement is that the electric fields from the individual antennas add coherently in the far field of the array. Meeting this requirement has two elements: (i) The delays to each antenna must be measured and any temporal changes (e.g., due to changing temperatures producing different electrical paths) must be monitored and compensated; and (ii) The relative Doppler shifts between the antennas must be removed, necessitating an ephemeris for the target.

Techniques for calibrating the delays for a (receive-only) radio astronomical array using a *reference emitter* are mature for radio astronomical (receive-only) arrays. In principle, for a radar array round-trip phase measurements could be conducted to monitor the delays to each antenna. However, it is generally difficult to measure the phase contributed by the feed or the horn at the antenna *and* the lines of sight from the different antennas through Earth's atmosphere can have differential delays. These difficulties have led to the concept of a *reference receiver*.

Different scenarios have been developed and demonstrated for a reference receiver, ranging from an elevated receiver mounted at some distance from the radar array [8] to using the Moon itself [39]. Crucially, these initial demonstrations have achieved the expected N^2 improvements for coherent addition of antennas and long-term stability of the calibration (Figure 6).

4.4 Siting

While Sánchez Net et al. [32] did not consider siting considerations in detail, a few general comments are warranted.

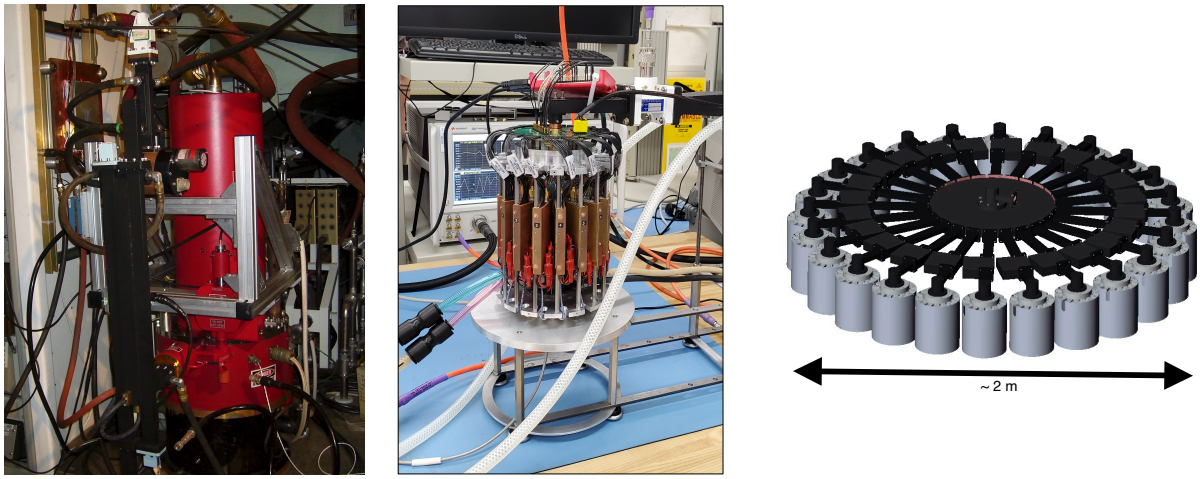

Fig. 5: Illustrations of the range of implementations and transmit powers that could be provided by the transmit subsystem within a planetary radar array. (*left*) Klystron (high-power microwave amplifier) that provides 80 kW of output power at a frequency near 7.2 GHz and is used for transmitting to spacecraft within NASA's Deep Space Network. For reference, the unit stands approximately 1.2 m tall. (*middle*) Prototype solid-state microwave amplifier that has been developed at JPL. This unit produces 1.1 kW of output power at frequencies near 8.56 GHz. This solid-state module consists of 16 solid-state 80 W monolithic microwave integrated circuit (MMIC) amplifiers, which are visible as the vertical boards. The outputs of the 16 amplifiers are combined to produce the 1.1 kW of output power through the wave guide at the top of the unit. For reference, this prototype unit is approximately 0.2 m tall. (*right*) Design of a 25 kW amplifier system composed of multiple solid-state units shown in the middle panel. This design uses radial combining and illustrates how the use of solid-state units enables a modular architecture.

First, a relatively compact array is desirable. For radio astronomical arrays, a prime motivation often is increased angular resolution, for which an interferometric array is the only feasible approach to obtaining the required angular resolutions. The result is that radio astronomy arrays typically have antenna separations of tens to hundreds of kilometers or larger. By contrast, rarely are the targets for radar arrays expected to be able to be resolved angularly. Further, on-going experiments at the Jet Propulsion Laboratory are confirming that maintaining the desired phasing for transmission is increasingly more difficult for radar arrays having separations between the antennas larger than a few kilometers.

In addition to being desirable from the perspective of calibration, a relatively compact array could make other infrastructure aspects (roads, power distribution, signal transport, ...) less expensive. Additional cost savings may be possible by siting a planetary radar array near another facility that already has some of these infrastructure aspects present.

A mid-latitude arid site is likely optimum. For planetary science and defense considerations, a site located as close to the equator as possible is desirable in order to maximize the fraction of the sky visible. In addition, if one of the objectives is safety and mission assurance for lunar orbiting spacecraft, sites at latitudes $|b| > 30^\circ$ would have the risk that the Moon is not visible throughout its orbit. However, the characteristics of the ionosphere at equatorial latitudes may make observations more difficult at times. This risk can be mitigated somewhat by choosing frequencies sufficiently high that the effects of the ionosphere are not significant, but, at increasingly higher frequencies, the amount of water vapor in the troposphere can become significant. Notably, Table 2 shows that the current and proposed radar transmitters have operational frequencies of about 7 GHz to 15 GHz (or IEEE radar bands of C band to K_u band); the Arecibo Observatory transmitted at 2.38 GHz (S band). These frequencies are in the range such that neither the ionosphere nor the troposphere introduce significant corruptions to observations.

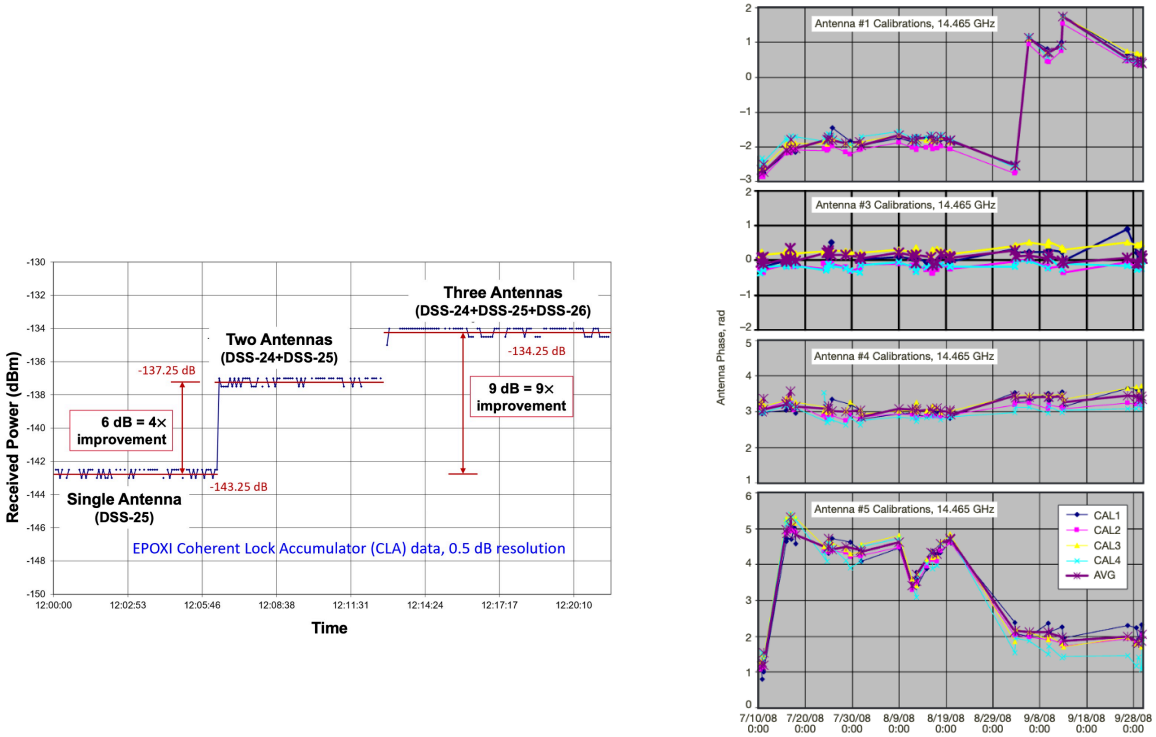

Fig. 6: Demonstrations of the calibration of an array of transmitting antennas (cf. Figure 4). (*left*) Illustration of successful calibration of a three-element array experiment with the DSN. (From Vilnrotter et al. [38]) Shown is the received power at the Extrasolar Planet Observation and Deep Impact Extended Investigation (EPOXI) spacecraft as a function of time. From 12:00 to approximately 12:06, only a single antenna (DSS-25) was transmitting; at approximately 12:06, a second antenna was added, forming a two-element array (DSS-24+DSS-25), with the expected 6 dB (4×) improvement in received power resulting; and, at approximately 12:13, a third antenna was added (DSS-24+DSS-25+DSS-26), with the expected 9.5 dB (9×) improvement in received power resulting relative to the single-antenna case. (*right*) Demonstration of the system stability for an array of transmitting antennas, from the Loop Canyon array. (From D'Addario et al. [7]) Shown is the phase of four of the antennas in array relative to Antenna 2 as a function of time. Phase stability (in a root-mean-square sense) of better than 0.1 radians could be maintained over intervals of days to weeks. (The cause of the phase jump at Antenna 1 near 2008 September 8 was not established.)

4.5 System Optimization

Sánchez Net et al. [32] show that a figure of merit for a radar array can be expressed as

$$\mathrm{FOM} = \underbrace{\frac{\pi\eta}{4^3\lambda^2 k_B T_{\mathrm{sys}}}}_{\text{constant}} \cdot \underbrace{N^3 P_a D_a^4}_{\text{system factor}} \cdot \underbrace{\frac{\sigma}{R^4}\sqrt{\frac{\Delta t}{B}}}_{\text{target factor}}. \tag{3}$$

An underlying assumption for this figure of merit is that monostatic operations are intended, i.e., the same array is used for both transmission and reception, a point to which we return below.

constant This first factor consists of fundamental constants and factors that can be considered to be uniform throughout the radar array. Many of these factors are evident in eqns. (1) and (2) and the subsequent discussion. Here η is an efficiency factor capturing several loss factors, such as inefficiencies in phasing the array or incomplete illumination of the antennas, with an illustrative value being $\eta \approx 0.70$.

system factor This second factor consists of the elements of the parameters of the model to be varied in seeking the optimum. Here N is the number of antennas, P_a is the power transmitted by each antenna, and D_a is the diameter of each antenna. Relative to eqn. (2), these terms can be understood as $P_{\mathrm{TX}} = NP_a$ and $G_{\mathrm{TX}} = G_{\mathrm{RX}} \propto ND_a^2$. In

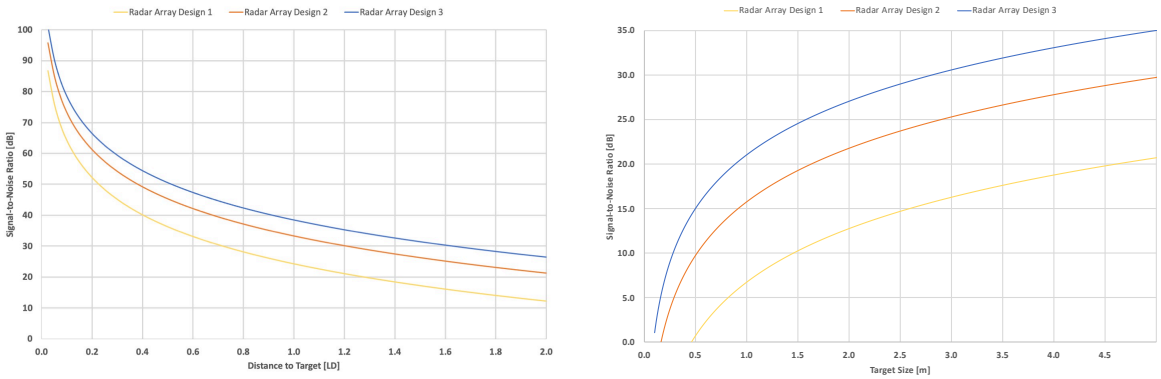

Fig. 7: Projected planetary radar array performance for an array composed of 15 m-diameter antennas, each with a 20 kW transmitter, based on the optimum found by Sánchez Net et al. [32]. (*left*) Signal-to-noise ratio (in dB) as a function of the distance (in units of lunar distance [LD]) to a 50 m-diameter asteroid having a typical radar albedo of 0.1. Illustrated are arrays of 5 × 15 m antennas (gold), 10 × 15 m antennas (orange), and 15 × 15 m antennas (blue), in all cases, each antenna in the array is equipped with a 20 kW transmitter. The projected performance would improve for a larger diameter asteroid or one with a larger radar albedo, and it would correspondingly diminish for an asteroid with a smaller diameter or smaller radar albedo. These projections assume that the asteroid is far from the Moon in angular separation (cf. Table 2). (*right*) Signal-to-noise ratio (in dB) for spacecraft of dimensions ranging from 10 cm (1U CubeSat) to 4 m (slightly larger than LRO), in all cases assuming a radar albedo of unity, a distance of 1 lunar distance, and a target far from the Moon in angular separation. Additional antennas would be required to compensate for pointing in directions close to the Moon; see the text for additional discussion. The curves show the same arrays as in the left panel.

Figure 6, only an N^2 improvement is shown because the receiving system was a single antenna (on the EPOXI spacecraft) rather than a radar array.

target factor This third factor contains parameters that describe characteristics of the target. Here, its radar cross section is σ, the integration time on target is Δt, the Doppler bandwidth B is related to the rotational period of the target (§3), and R is the range to the target.

Sánchez Net et al. [32] modeled the cost function for a radar array as having two major contributions, one from the *implementation* $C_{\rm impl}$ and one from the *operations and maintenance* $C_{\rm ops}$.

$$\begin{aligned} C_{\rm impl} &\propto (C_a + C_{\rm trans}) N^{1-\gamma_n}; \\ C_{\rm ops} &= N C_{\rm element} + C_{\rm fixed}. \end{aligned} \tag{4}$$

Here C_a is the cost of an individual antenna element, *excluding the cost of its transmitting system*, and $C_{\rm trans}$ is the cost of an individual transmitting system. The implementation cost factor clearly increases with the number of antennas N, but the factor γ_n reflects a "learning factor" related to economies of scale if N becomes sufficiently large. Meanwhile, the operations cost function attempts to capture both costs that scale clearly with the number of antennas N and those costs $C_{\rm fixed}$ that are (essentially) insensitive to the number of antennas. This cost function model is shown to replicate the estimated implementation and operations costs of the 25-element VLA to better than 10%.

Figure 7 projects the capabilities of a planetary radar array, both for the purposes of planetary science and defense and for safety and mission assurance. The array parameters illustrated (15 m-diameter antennas, 20 kW transmitters) is based the optimum found by Sánchez Net et al. [32], but similar performance is projected for arrays with comparable parameters.

Crucially, this analysis assumes a target located far from the Moon in angular distance (cf. Table 2). From eqns. (2) and (3), pointing close to the Moon increases the system temperature $T_{\rm sys}$ in the receiving system such that the gain of the receiving system $G_{\rm RX}$, and ultimately the number of antennas in the array N, must be increased. A typical increase in $T_{\rm sys}$ due to pointing close to the Moon might be 10× (from approximately 25 K far from the Moon to approximately

250 K close to the Moon). Accordingly, the required number of antennas would be increased by a factor of at least two, and more likely closer to three in order to provide margin. Thus, the required number would be 45 antennas. Even so, this number of antennas is comparable to the number in currently operational radio astronomcial arrays and relatively modest compared to the hundreds of antennas planned for near-future radio astronomical arrays, though a planetary radar array also requires a high-power transmitter at each antenna.

5. SUMMARY

The current suite of ground-based planetary radar assets has and continues to produce an impressive suite of discoveries, has been critical to the planning of various robotic missions by providing precise orbits, and is a crucial element of planetary defense activities by providing precise orbits and characterizations of near-Earth asteroids (NEAs). While the primary focus has been on planetary science, which includes planetary defense, the NASA Goldstone Solar System Radar (GSSR) also has contributed to safety and mission assurance assessments by contributing to measurements of orbital debris.

We have illustrated how these techniques for safety and mission assurance can begin to be extended to the cislunar arena. While planetary radar observations of NEAs that are at distances of approximately 1 lunar distance have been conducted for some time, these observations typically occur far from the Moon in angular separation. Of particular note for planetary radar observations for safety and mission assurance in the cislunar arena is the reduction in the sensitivity of receiving systems for radar return signals. We suggest that there are multiple "use cases," depending upon the angle between the target and the Moon, and, all other factors being equal, the performance of a planetary radar system will be degraded the closer it has to point toward the Moon.

We have summarized maturing technologies that would enable a new planetary radar capability, based on an array of multiple antennas forming a *planetary radar array*. The use of an array of antennas for reception of signals is a well-demonstrated technology in radio astronomy, and there have been a number of initial demonstrations of the arrays of antennas for the purposes of deep space communication and planetary radar.

Acknowledgments We thank L. D'Addario for helpful comments. Part of this research was carried out at the Jet Propulsion Laboratory, California Institute of Technology, under a contract with the National Aeronautics and Space Administration. The National Radio Astronomy Observatory is a facility of the National Science Foundation operated under cooperative agreement by Associated Universities, Inc. The Australia Telescope Compact Array (ATCA) is part of the Australia Telescope National Facility[9] which is funded by the Australian Government for operation as a National Facility managed by CSIRO. We acknowledge the Gomeroi people as the traditional owners of the Observatory site. The authors acknowledge ideas and advice from the participants in the Next-Generation Ground-Based Planetary Radar workshop organized by the W.M. Keck Institute for Space Studies.

[9] https://ror.org/05qajvd42

[1] Craig Benson, John Reynolds, N. J. S. Stacy, Lance A. M. Benner, P. G. Edwards, Graham Baines, Russell Boyce, Jon D. Giorgini, Joseph S. Jao, George Martinez, Martin A. Slade, Lawrence P. Teitelbaum, Aseel Anabtawi, Daniel Kahan, Kamal Oudrhiri, C. J. Philips, J. B. Stevens, Ed Kruzins, and T. Joseph W. Lazio. First Detection of Two Near-Earth Asteroids With a Southern Hemisphere Planetary Radar System. *Radio Science*, 52(11):1344–1351, November 2017.

[2] M. Brozović, B. J. Butler, J. Margot, S. P. Naidu, and T. J. W. Lazio. Planetary Bistatic Radar. In Eric Murphy, editor, *Science with a Next Generation Very Large Array*, volume 517 of *Astronomical Society of the Pacific Conference Series*, page 113, December 2018.

[3] M. Brozović, R. S. Park, J. G. Mcmichael, J. D. Giorgini, M. A. Slade, D. S. Berry, J. S. Jao, F. D. Ghigo, P. A. Taylor, and E. Rivera-Valentín. Radar observations of spacecraft in lunar orbit. In 26th *International Symposium on Space Flight Dynamics*, 2017. ISTS-2017-d-107/ISSFD-2017-107.

[4] J. Bunton. Memo 90: Dish cost frequency scaling. Technical report, Square Kilometer Array, 2007.

[5] Michael W. Busch, Shrinivas R. Kulkarni, Walter Brisken, Steven J. Ostro, Lance A. M. Benner, Jon D. Giorgini, and Michael C. Nolan. Determining asteroid spin states using radar speckles. *Icarus*, 209(2):535–541, October 2010.

[6] Michael W. Busch, Steven J. Ostro, Lance A. M. Benner, Marina Brozovic, Jon D. Giorgini, Joseph S. Jao, Daniel J. Scheeres, Christopher Magri, Michael C. Nolan, Ellen S. Howell, Patrick A. Taylor, Jean-Luc Margot, and Walter Brisken. Radar observations and the shape of near-Earth ASTEROID 2008 EV5. *Icarus*, 212(2):649–660, April 2011.

[7] L. D'Addario, R. Proctor, J. Trinh, E. Sigman, and C. Yamamoto. Uplink Array Demonstration with Ground-Based Calibration. *Interplanetary Network Progress Report*, 42-176:1–69, February 2009.

[8] L. R. D'Addario. Combining Loss of a Transmitting Array due to Phase Errors. *Interplanetary Network Progress Report*, 42-175:1–7, November 2008.

[9] I. de Pater, P. Palmer, D. L. Mitchell, S. J. Ostro, D. K. Yeomens, and L. E. Snyder. Radar aperture synthesis observations of asteroids. *Icarus*, 111:489–502, October 1994.

[10] M. Di Martino, S. Montebugnoli, G. Cevolani, S. Ostro, A. Zaitsev, S. Righini, L. Saba, S. Poppi, M. Delbò, A. Orlati, G. Maccaferri, C. Bortolotti, A. Gavrik, and Y. Gavrik. Results of the first Italian planetary radar experiment. *Planet. Space Sci.*, 52(4):325–330, March 2004.

[11] Jon D. Giorgini, Lance A. M. Benner, Marina Brozović, Michael W. Busch, Donald B. Campbell, Steven R. Chesley, Paul W. Chodas, Ellen Howell, Jean-Luc Margot, Andrea Milani, Petr Pravec, Robert A. Preston, Maria-Eugenia Sansaturio, Daniel J. Scheeres, Michael K. Shepard, Arnold Silva, Martin A. Slade, Patrick A. Taylor, Giovanni Valsecchi, David Vokrouhlicky, and Donald K. Yeomans. Radar Astrometry of Small Bodies: Detection, Characterization, Trajectory Prediction, and Hazard Assessment. Technical report, Jet Propulsion Laboratory, National Aeronautics and Space Administration, 2009b. White Paper, submitted to the Planetary Sciences Decadal Survey (2013–2022).

[12] R. M. Goldstein and Jr. Goldstein, S. J. Flux of Millimetric Space Debris. *Astron. J.*, 110:1392, September 1995.

[13] Shinji Horiuchi, Blake Molyneux, Jamie B. Stevens, Graham Baines, Craig Benson, Zohair Abu-Shaban, Jon D. Giorgini, Lance A. M. Benner, Shantanu P. Naidu, Chris J. Phillips, Philip G. Edwards, Ed Kruzins, Nick J. S. Stacy, Martin A. Slade, John E. Reynolds, and Joseph Lazio. Bistatic radar observations of near-earth asteroid (163899) 2003 SD220 from the southern hemisphere. *Icarus*, 357:114250, March 2021.

[14] A. W. Hotan, J. D. Bunton, A. P. Chippendale, M. Whiting, J. Tuthill, V. A. Moss, D. McConnell, S. W. Amy, M. T. Huynh, J. R. Allison, C. S. Anderson, K. W. Bannister, E. Bastholm, R. Beresford, D. C. J. Bock, R. Bolton, J. M. Chapman, K. Chow, J. D. Collier, F. R. Cooray, T. J. Cornwell, P. J. Diamond, P. G. Edwards, I. J. Feain, T. M. O. Franzen, D. George, N. Gupta, G. A. Hampson, L. Harvey-Smith, D. B. Hayman, I. Heywood, C. Jacka, C. A. Jackson, S. Jackson, K. Jeganathan, S. Johnston, M. Kesteven, D. Kleiner, B. S. Koribalski, K. Lee-Waddell, E. Lenc, E. S. Lensson, S. Mackay, E. K. Mahony, N. M. McClure-Griffiths, R. McConigley, P. Mirtschin, A. K. Ng, R. P. Norris, S. E. Pearce, C. Phillips, M. A. Pilawa, W. Raja, J. E. Reynolds, P. Roberts, D. N. Roxby, E. M. Sadler, M. Shields, A. E. T. Schinckel, P. Serra, R. D. Shaw, T. Sweetnam, E. R. Troup, A. Tzioumis, M. A. Voronkov, and T. Westmeier. Australian square kilometre array pathfinder: I. system description. *Publ. Astron. Soc. A*, 38:e009, March 2021.

[15] J. Jonas and MeerKAT Team. The MeerKAT Radio Telescope. In *MeerKAT Science: On the Pathway to the SKA*, page 1, January 2016.

[16] D. Jones and J. Lazio. Enhancing Science from Future Space Missions and Planetary Radar with the SKA. In *Advancing Astrophysics with the Square Kilometre Array (AASKA14)*, page 154, April 2015.

[17] C. G. Lee, M. A. Slade, J. S. Jao, and N. Rodriguez-Alvarez. Micro-meteoroid and orbital debris radar from goldstone radar observations. In *First International Orbital Debris Conference*. Lunar & Planetary Institute, 2019. https://www.hou.usra.edu/meetings/orbitaldebris2019/orbital2019paper/pdf/6185.pdf.

[18] Bruce E MacNeal and WJ Hurd. Parametric cost analysis of nasa's dsn array. In *Space OPS 2004 Conference*, page 433, 2004.

[19] M. J. Matney and E. Stansbery. What are radar observations telling us about the low-earth orbital debris environment? In *Third European Conference on Space Debris*, 2001.

[20] D. D. Morabito. Lunar Noise-Temperature Increase Measurements at S-Band, X-Band, and Ka-Band Using a 34-Meter-Diameter Beam-Waveguide Antenna. *Interplanetary Network Progress Report*, 42-166:1–18, August 2006.

[21] D. D. Morabito. Dynamic Telemetry Link Advantage When Tracking a Lunar Orbiter with a 34-m Antenna at 2.3 GHz and 8.4 GHz. *Interplanetary Network Progress Report*, 42-200:1–17, February 2015.

[22] D. O. Muhleman, B. J. Butler, A. W. Grossman, and M. A. Slade. Radar images of Mars. *Science*, 253:1508–1513, September 1991.

[23] D. O. Muhleman, A. W. Grossman, B. J. Butler, and M. A. Slade. Radar reflectivity of Titan. *Science*, 248:975–980, May 1990.

[24] S. P. Naidu, L. A. M. Benner, J.-L. Margot, M. W. Busch, and P. A. Taylor. Capabilities of Earth-based Radar Facilities for Near-Earth Asteroid Observations. *Astron. J.*, 152(4):99, October 2016.

[25] Toshihaya Nakahara, Youhei Yamada, Toshiya Otake, Hiroyuki Asao, Kenji Izukura, and Kousuke Kohigashi. Development of 30 kw-class x-band solid state power amplifier for the misasa deep space station. *NEC Technical Journal*, 16(1), 2021. Special Issue on Social Infrastructure that Guarantees Safety, Security, Fairness, and Efficiency.

[26] M. Nechaeva, A. Antipenko, D. Bezrukov, Vl. Bezrukovs, A. Dementjev, N. Dugin, N. Jekabsons, R. Khutornoy, M. Klapers, A. Konovalenko, V. Kulishenko, A. Nabatov, V. Nesteruk, G. Pupillo, A. Reznichenko, E. Salerno, I. Shmeld, K. Skirmante, Yu. Tikhomirov, and V. Voytyuk. First Results of the VLBI Experiment on Radar Location of the Asteroid 2012 DA14. *Baltic Astronomy*, 22:341–346, January 2013.

[27] S. J. Ostro. Planetary radar astronomy. *Rev. Modern Phys.*, 65(4):1235–1279, October 1993.

[28] S. J. Ostro. Planetary radar astronomy. In R. A. Meyers, editor, *Encyclopedia of Physical Science and Technology*, pages 295–328. Academic Press, New York, third edition edition, 2003. ISBN: 978-0-12-227410-7.

[29] S. J. Ostro. *Encyclopedia of the Solar System*, chapter Planetary Radar, pages 735–764. Elsevier, Inc., 2nd edition edition, 2007.

[30] S. J. Ostro, R. S. Hudson, L. A. M. Benner, J. D. Giorgini, C. Magri, J. L. Margot, and M. C. Nolan. Asteroid Radar Astronomy. In W. F. Bottke Jr., A. Cellino, P. Paolicchi, and R. P. Binzel, editors, *Asteroids III*, pages 151–168. Univ. Arizona Press, 2002.

[31] Steven J. Ostro and Jon D. Giorgini. The role of radar in predicting and preventing asteroid and comet collisions with Earth. In Michael J. S. Belton, Thomas H. Morgan, Nalin H. Samarasinha, and Donald K. Yeomans, editors, *Mitigation of Hazardous Comets and Asteroids*, page 38, January 2004.

[32] M. Sánchez Net, M. Taylor, V. Vilnrotter, and T. J. W. Lazio. A ground-based planetary radar array. *The Interplanetary Network Progress Report*, 42-229:1–31, May 2022. https://ipnpr.jpl.nasa.gov/progress_report/42-229/42-229A.pdf.

[33] R.T. Schilizzi, P. Alexander, and J.M. Cordes. Memo 100: Preliminary specification for the square kilometre array. Technical report, Square Kilometer Array, 2007.

[34] R. Selina. System-level evaluation of aperture size. Technical report, Next Generation Very Large Array, 2019.

[35] M. A. Slade, B. J. Butler, and D. O. Muhleman. Mercury radar imaging - Evidence for polar ice. *Science*, 258:635–640, October 1992.

[36] JI Statman, DS Bagri, CS Yung, S Weinreb, and BE MacNeal. Optimizing the antenna size for the deep space network array. *Interplanetary Network Progress Report*, pages 1–8, 2004.

[37] V. Vilnrotter, D. Lee, T. Cornish, R. Mukai, and L. Paal. Uplink Arraying Experiment with the Mars Global Surveyor Spacecraft. *Interplanetary Network Progress Report*, 42-166:1–14, August 2006.

[38] V. Vilnrotter, D. Lee, T. Cornish, P. Tsao, L. Paal, and V. Jamnejad. Uplink array concept demonstration with the EPOXI spacecraft. In *2009 IEEE Aerospace Conference*, pages 1–8, 2009.

[39] V. Vilnrotter, D. Lee, T. Cornish, P. Tsao, L. Paal, and V. Jamnejad. Uplink array concept demonstration with the EPOXI spacecraft. *IEEE Aerospace and Electronic Systems Magazine*, 25(5):29–35, May 2010.

[40] V Vilnrotter, D Lee, P Tsao, T Cornish, and L Paal. Uplink array calibration via lunar doppler-delay imaging. In

2010 IEEE Aerospace Conference, pages 1–12. IEEE, 2010.

[41] V. Vilnrotter, P. Tsao, D. Lee, T. Cornish, J. Jao, and M. Slade. Planetary radar imaging with the Deep-Space Network's 34 meter Uplink Array. In *2011 Aerospace Conference*, pages 1–13. IEEE, 2011.

[42] Steven R. Wilkinson, Charlie Hansen, Barry Alexia, Bishara Shamee, Brian Lloyd, Anthony Beasley, Walter Brisken, Flora Paganelli, Galen Watts, Karen O'Neil, and Patrick Courtney. A planetary radar system for detection and high-resolution imaging of nearby celestial bodies. *Microwave J.*, 65, January 2022. https://www.microwavejournal.com/articles/37417-a-planetary-radar-system-for-detection-and-high-resolution-imaging-of-nearby-celestial-bodies.